Supplementary Methods

"Seasonal evolution of supraglacial lakes on a floating ice tongue, Petermann Glacier, Greenland"

Grant J. Macdonald, Alison F. Banwell and Douglas R. MacAyeal

Methods

1. Lake boundary/area algorithm

The lake boundary/area algorithm (Box and Ski, 2007; Banwell and others, 2014) creates a mask of SGL areas by classifying the image pixels as either 'water-covered' or not. OLI bands 2 (blue; 450-510 nm) and 4 (red; 640-670 nm) were first converted from digital numbers to reflectance values using the equations of Chander and others (2009). Then the blue/red ratio of reflectance was evaluated; this ratio is highest where water is darkest in colour, indicative of deep water, and decreases towards the shallower lake edge. Based on testing different blue/red ratios and visual comparison with the pan-sharpened true-color images, a single minimum-threshold ratio, corresponding to the lake edge, was selected to identify the lakes throughout the season. A threshold ratio of 1.5 was chosen for this study, which is the same as that chosen by Pope and others (2016), and is comparable to threshold values used by Banwell and others (2014; 1.05-1.25) and Arnold and others (2014; 2-3). Sensitivity tests indicated that application of a threshold ratio > 1.5 excluded too many SGLs that were otherwise visible by manual visual interpretation, and a threshold ratio < 1.5 identified too many false-positives. An exception was made for the higher-elevation Site 4 (location shown in Fig. 1) in objective (iii) only, where it was found to be necessary to use a higher threshold value of 1.9 to avoid classifying large expanses of slush as SGLs (Yang and Smith, 2013). The nature of the identification algorithm means that lakes with a complete snow- and/or ice-cover were not identified as SGLs.

Following Pope and others (2016), water-covered features identified by the algorithm that were ≤ 4 pixels in area were removed. A threshold of 4 was deemed

sufficiently high to exclude small features that likely comprised solely of mixed pixels (i.e. those with a value representative of the average of different surface types, e.g. snow/ice/water) while being sufficiently low to maximize inclusion of small lakes. However, unlike the study by Pope and others (2016), which did not classify any water-covered features narrower than 2 pixels (i.e. 60 m) as SGLs, we decided to classify these areas as SGLs. This decision was based on manual visual interpretation of the study site in pan-sharpened (15 m spatial resolution) OLI imagery that indicated that many of these narrow features, particularly on the low surface-gradient tongue, are SGLs, and not meltwater channels. This does mean, however, that some sections of channels may have been misidentified as SGLs in our analysis.

Some shadows on the ice tongue - due to large- and small-scale nearby topography - were also found to cause false-positives in some instances. For example, a 2.6 km^2 area on the western flank of the tongue was persistently covered in shadow from the fjord walls and thus was excluded from analysis. Variations in the surface topography of the tongue, particularly towards the end of each melt season, cast small, localized, shadows that were falsely identified as SGLs. These features were difficult to identify and quantify for exclusion and therefore contribute to noise and uncertainty in our analysis.

2. Lake-depth algorithm

Following Banwell and others (2014), with improvements suggested by Pope and others (2016), we employed the lake-depth algorithm originally based on the Beer-Lambert law (Ingle and Crouch, 1988) and developed by Sneed and Hamilton (2007), which describes the attenuation of radiation through a water column. The depth of a SGL can be approximated as

$$z = [\ln(A_d - R_\infty) - \ln(R_{lake} - R_\infty)]/g$$

where z is lake depth in meters, A_d is the lake bottom albedo, R_∞ is the reflectance of optically deep water, R_{lake} is the reflectance of a lake pixel, and g is a value related to the losses in upward and downward travel through the water column and varies

with the wavelength used. To determine A_d, the mean reflectance of a ring of pixels adjacent to the identified SGL pixels was assumed to be representative of the pixels at the lake bottom. Some images did not contain optically deep water, and the difference in results between using an R_∞ value of 0 and a value obtained from the ocean (as in Banwell and others, 2014) was found to be negligible. Therefore, an R_∞ value of 0 was used and considered sufficiently accurate for the purposes of the study. g values were taken from Pope and others (2016).

The depth of each pixel in a SGL was calculated using a measure of reflectance both in band 2 and band 8 (panchromatic; 520-900 nm), and the final depth result was taken as the mean of the two results, as recommended by Pope and others (2016) for OLI imagery.

The lake depth algorithm makes several assumptions. It assumes that: i) the substrate of the lake is homogenous and that the impact on absorption of any dissolved matter in the water is negligible; ii) there is no scattering of light from the lake surface associated with roughness due to wind; and iii) that the albedo of the pixels at the edge of lake is representative of those at the lake bottom (Sneed and Hamilton, 2007; Banwell and others, 2014).

Supplementary references

Chander G., B. L. Markham and D. L. Helder (2009) Summary of current radiometric calibration coefficients for Landsat MSS, TM, ETM+, and EO-1 ALI sensors, *Remote Sens. Environ.*, **113**(5), 893–903 (doi: 10.1016/j.rse.2009.01.007)

Ingle, J. D. and S. R. Crouch (1988) Spectrochemical measurements. In: *Spectrochemical analysis* (eds. Ingle, J. D. and S. R. Crouch) Prentice Hall, Upper Saddle River, NJ

Yang, K. and L. C. Smith (2013) Supraglacial streams on the Greenland Ice Sheet Delineated From Combined Spectral-Shape Information in High-Resolution Satellite Imagery, *IEEE Geosci. & Rem. Sens. Lett.*, **10**(4), 801-805 (doi: 10.1109/LGRS.2012.2224316)

Supplementary figures

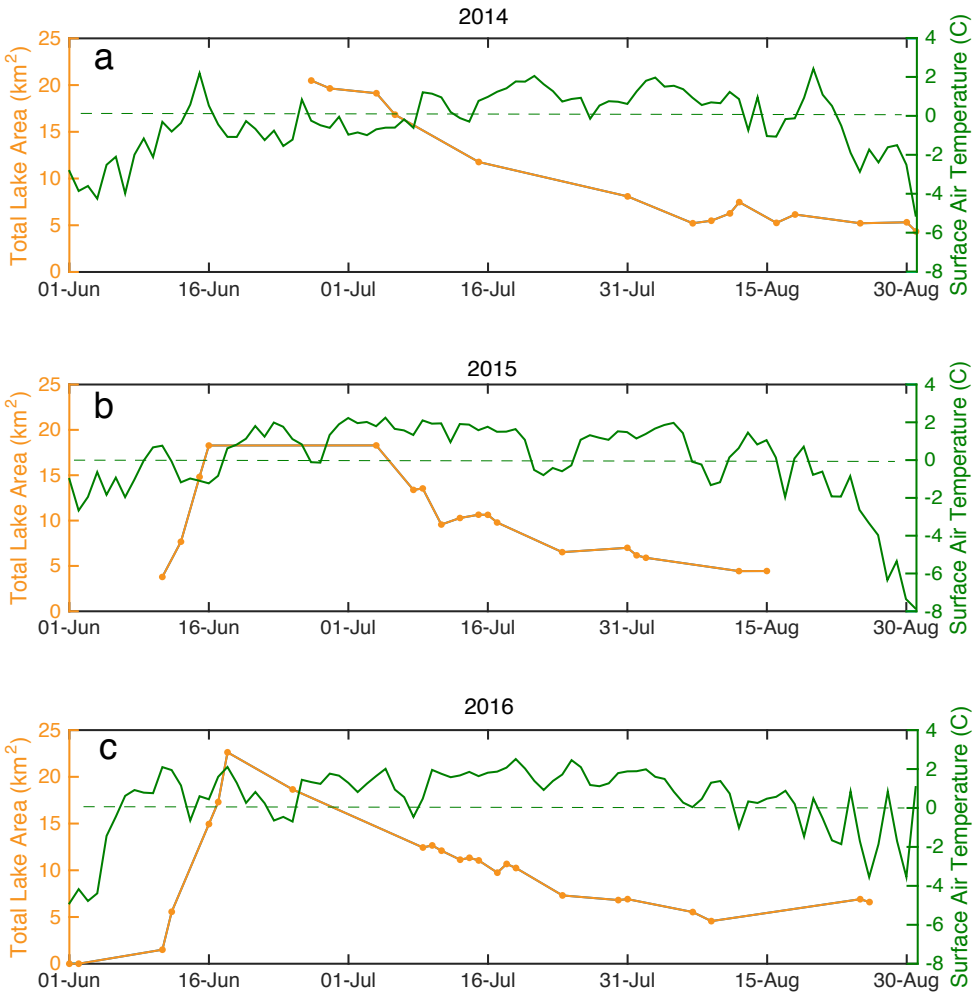

Fig. S1. Variations in total lake area (TLA, orange) and daily mean surface air temperature (green) on Petermann's floating tongue in (a) 2014, (b) 2015 and (c) 2016.

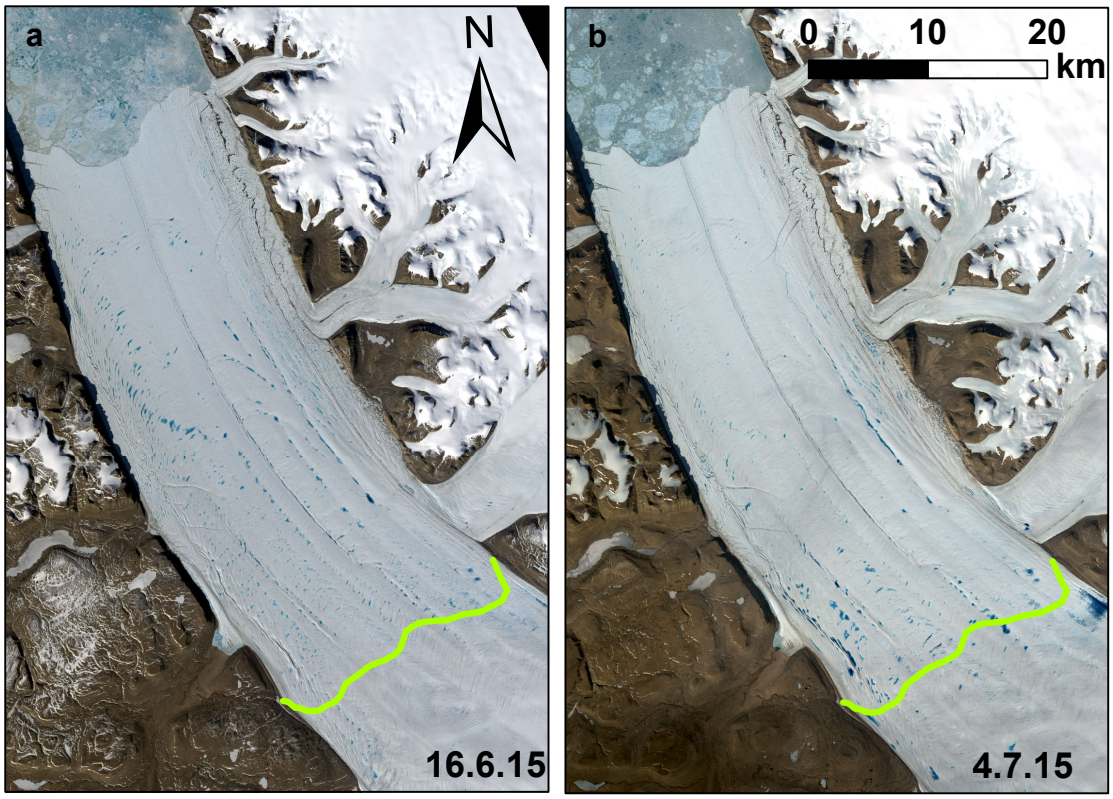

Fig. S2. The floating tongue on (a) 16 June and (b) 4 July 2015 in pan-sharpened OLI images. Note the increase in SGL coverage close to the grounding line (green) between the images, while many SGLs closer to the terminus have drained.

Supplementary tables

(a) Seasonal evolution of SGLs: 2014	
Date	**Image ID**
27 June	LC80312482014178LGN00
29 June	LC80450012014180LGN00
4 July	LC80642432014185LGN00
6 July	LC80302482014187LGN00
15 July	LC80450012014196LGN00
31 July	LC80612432014212LGN00
7 August	LC80302482014219LGN00
9 August	LC80440012014221LGN00
11 August	LC80420012014223LGN00
12 August	LC80652432014224LGN00
16 August	LC80450012014228LGN00
18 August	LC80430012014230LGN00
25 August	LC80440012014237LGN00
30 August	LC80312482014242LGN00
31 August	LC80380022014243LGN00

(b) Seasonal evolution of SGLs: 2015	
Date	**Image ID**
11 June	LC80420012015162LGN00
13 June	LC80400012015164LGN00
15 June	LC80380022015166LGN00
16 June	LC80450012015167LGN00
4 July	LC80430012015185LGN00
8 July	LC80390012015189LGN00
9 July	LC80302482015190LGN00
11 July	LC80440012015192LGN00
13 July	LC80420012015194LGN00
15 July	LC80400012015196LGN00
16 July	LC80312482015197LGN00
17 July	LC80380022015198LGN00
24 July	LC80390022015205LGN01
31 July	LC80400012015212LGN00
1 August	LC80312482015213LGN00
2 August	LC80380022015214LGN00
12 August	LC80440012015224LGN00
14 August	LC80420012015226LGN00

(c) Seasonal evolution of SGLs: 2016	
Date	**Image ID**
1 June	LC80380022016153LGN00
2 June	LC80450012016154LGN00
11 June	LC80440012016163LGN00
12 June	LC80672422016164LGN00
16 June	LC80632432016168LGN00
17 June	LC80380022016169LGN00
18 June	LC80612432016170LGN00
25 June	LC80622432016177LGN00
9 July	LC80642432016191LGN00
10 July	LC80390012016192LGN00
11 July	LC80622432016193LGN00
13 July	LC80440012016195LGN00
14 July	LC80672422016196LGN00
15 July	LC80420012016197LGN00
17 July	LC80400012016199LGN00
18 July	LC80632432016200LGN00
19 July	LC80380022016201LGN00
24 July	LC80410012016206LGN00
30 July	LC80672422016212LGN00
31 July	LC80420012016213LGN00
7 August	LC80430012016220LGN00
9 August	LC80410012016222LGN00
25 August	LC80410012016238LGN00
26 August	LC80322482016239LGN00

Table S1. Table of satellite image IDs and dates used in the analysis of intra- and inter-seasonal evolution of SGLs in (a) 2014, (b) 2015 and (c) 2016 (objective i)

(a) Seasonal evolution of individual SGLs: Lake A	
Date	**Image ID**
Year: 2014	
17 June	LC80410012014168LGN00
20 June	LC80302482014171LGN00
24 June	LC80420012014175LGN00
25 June	LC80652432014176LGN00
26 June	LC80400012014177LGN00
Year: 2015	
11 June	LC80420012015162LGN00
13 June	LC80400012015164LGN00
15 June	LC80380022015166LGN00
16 June	LC80450012015167LGN00
Year: 2016	
11 June	LC80440012016163LGN00
12 June	LC80672422016164LGN00
16 June	LC80632432016168LGN00
17 June	LC80380022016169LGN00
18 June	LC80612432016170LGN00
25 June	LC80622432016177LGN00

(b) Seasonal evolution of individual SGLs: Lake B	
Date	**Image ID**
Year: 2014	
17 June	LC80410012014168LGN00
20 June	LC80302482014171LGN00
24 June	LC80420012014175LGN00
25 June	LC80652432014176LGN00
26 June	LC80400012014177LGN00
27 June	LC80632432014178LGN00
29 June	LC80450012014180LGN00
30 June	LC80360022014181LGN00
1 July	LC80430012014182LGN00
4 July	LC80642432014185LGN00
5 July	LC80390012014186LGN00
6 July	LC80302482014187LGN00
15 July	LC80450012014196LGN00
Year: 2015	
11 June	LC80420012015162LGN00
13 June	LC80400012015164LGN00
15 June	LC80380022015166LGN00
16 June	LC80450012015167LGN00
4 July	LC80430012015185LGN00
8 July	LC80390012015189LGN00
9 July	LC80302482015190LGN00
11 July	LC80440012015192LGN00
13 July	LC80420012015194LGN00
15 July	LC80400012015196LGN00
16 July	LC80312482015197LGN00
17 July	LC80380022015198LGN00
24 July	LC80390022015205LGN01
31 July	LC80400012015212LGN00
1 August	LC80312482015213LGN00
Year: 2016	
16 June	LC80632432016168LGN00
17 June	LC80380022016169LGN00
18 June	LC80612432016170LGN00
25 June	LC80622432016177LGN00
9 July	LC80642432016191LGN00

Table S2. Table of satellite image IDs and dates used in the analysis of intra- and inter-seasonal evolution (a) Lake A and (b) Lake B (2014-2016) (objective ii)